UNIVERSITY
OF TRENTO

DIPARTIMENTO DI INGEGNERIA E SCIENZA DELL'INFORMAZIONE

38123 Povo – Trento (Italy), Via Sommarive 14
http://www.disi.unitn.it

OPTIMAL SUB-ARRAYING OF COMPROMISE PLANAR ARRAYS THROUGH AN INNOVATIVE ACO-WEIGHTED PROCEDURE

G. Oliveri and L. Poli

January 2011

Technical Report # DISI-11-011

Optimal Sub-arraying of Compromise Planar Arrays through an Innovative ACO-Weighted Procedure

G. Oliveri and L. Poli

ELEDIA Research Group

Department of Information Engineering and Computer Science,

University of Trento, Via Sommarive 14, 38123 Trento - Italy

Tel. +39 0461 882057, Fax +39 0461 882093

E-mail: {*giacomo.oliveri*, *lorenzo.poli*}@*disi.unitn.it*

Web-site: *http://www.eledia.ing.unitn.it*

Optimal Sub-arraying of Compromise Planar Arrays through an Innovative ACO-Weighted Procedure

G. Oliveri and L. Poli

Abstract

In this paper, the synthesis of sub-arrayed monopulse planar arrays providing an optimal sum pattern and best compromise difference patterns is addressed by means of an innovative clustering approach based on the Ant Colony Optimizer. Exploiting the similarity properties of optimal and independent sum and difference excitation sets, the problem is reformulated into a combinatorial one where the definition of the sub-array configuration is obtained through the search of a path within a weighted graph. Such a weighting strategy allows one to effectively sample the solution space avoiding bias towards sub-optimal solutions. The sub-array weight coefficients are then determined in an optimal way by exploiting the convexity of the problem at hand by means of a convex programming procedure. Representative results are reported to assess the effectiveness of the weighted global optimization and its advantages over previous implementations.

Key words: Sum and Difference Patterns Synthesis, Monopulse Antennas, Planar Arrays, Ant Colony Optimization, Convex Programming.

1 Introduction

Monopulse radars present several advantages over other search-and-track systems [1] based on conical scan or lobe switching approaches [2]. Indeed, tracking the angular positions of high-speed targets is enabled just processing a single pulse echo (a *monopulse*). Moreover, range measurements are generally more reliable because of echo signals with higher signal-to-noise ratios are dealt with, the sum beam being always directed towards the target. Monopulse radars require the generation of one sum pattern and a couple of spatially-orthogonal difference patterns to track targets both in azimuth and elevation [3]. Several implementations exploit reflectors or lens antennas [2], even if antenna arrays turn out to be more convenient for technological (e.g., the main beam can be electronically steered), implementative (e.g., heavy structures as reflectors are avoided), and applicative (e.g., arrays can be made conformal and installed on aircrafts) reasons. However, the complexity of the underlying beamforming network (BFN) must be properly taken into account since it unavoidably grows because of the need to generate more than one pattern and to use a large number of elements. To overcome these limitations, sub-arraying strategies (e.g., sub-array weighting [4] and overlapped sub-arrays [5]) as well as sharing common weights between the sum and difference channels [6][7] have been proposed. The sub-array weighting technique has received the widest interest as confirmed by the large number of published research works [8]-[17]. Generally, the problem is formulated as the synthesis of an optimal sum beam and the "best" compromise difference patterns grouping the array elements into suitably weighted sub-arrays. Towards this purpose, several optimization strategies have been applied. More specifically, the Simulated Annealing (SA) has been used in [8] to compute the sub-array weights for *a-priori* fixed element groupings, while a Genetic Algorithm (GA) [9] and two different implementations of the Difference Evolution (DE) algorithm [10][13] have been adopted to determine both weights and subarraying. Moreover, an effective hybrid method has been proposed in [11] to exploit the convexity of the problem with respect to the sub-array weights. Whether, on one hand, global optimization is mandatory to deal with the non-convex part of the problem, on the other, the "brute force" application of stochastic optimizers turns out being computationally

cumbersome and inefficient because of the exponential growth versus the number of array elements of the admissible sub-array configurations. Such a bottleneck has been efficiently solved in [18] by means of an excitation matching strategy where the sub-arraying grouping is "guided" by the similarity properties between the excitations providing the sum pattern and a set of reference excitations generating an optimal (reference) difference pattern. The dimension of the solution space has been significantly reduced and the final partitioning has been obtained by choosing $Q-1$ cut points (Q being the number of sub-arrays) in a sorted list of real values each one related to an antenna element. In such a way, the admissible set of sub-array configurations grows polynomially versus the number of elements with a non-negligible reduction of the solution space if compared to standard approaches. Furthermore, the *essential* solution space has been represented by means of a non-complete binary tree [18] and, successively, through a more compact and non-redundant direct acyclic graph (DAG) [19]. By virtue of its hill climbing behavior (mandatory for non-convex functionals), the Ant Colony Optimizer (ACO) [20] has been used to look for the optimal sub-array configuration both within the solution tree [21] as well as in the DAG [22]. Although the ACO has shown to outperform the ad-hoc deterministic method called Border Element Method (BEM) in both linear [18] and planar [19] problems, it still presents some inefficiencies when large-dimension problems as for planar architectures. It is worth pointing out that these drawbacks do not depend on the representation of the solution space or its dimension, but mainly on the control of the evolution process. Indeed, if all edges of the DAG have the same probability of being chosen at the initialization, some paths (i.e., sub-arraying solutions) turn out having less probability of being explored, while other paths are privileged. Such a bias is undesired and unavoidably limits the potentialities of the approach. On the other hand, although the non-complete binary tree [21] is not affected by such a drawback, it is not suitable for synthesizing large arrays because of high computational costs and memory storage requirements. In this work, a new synthesis approach based on an edge-weighting scheme is proposed to guarantee each path of the DAG be explored with an equal probability.

The rest of the paper is organized as follows. The synthesis problem is mathematically

formulated in Sect. 2 where the edge-weighting scheme for graph searching is presented, as well. Section 3 is devoted to the numerical analysis aimed at describing the behavior of the proposed approach and assessing its advantages and enhanced potentialities over previous implementations. Eventually, conclusions are drawn (Sect. 4).

2 Mathematical Formulation

Let us consider a monopulse planar array of $2M \times 2N$ elements displaced on a regular lattice with inter-element spacing d_x and d_y along the x and y axes, respectively. The antenna aperture is subdivided into four symmetrical quadrants whose outputs are combined to generate the sum and difference mode signals (Fig. 1) for the estimation of the off-boresight angle (OBA), namely the direction of the target with respect to the electrical axis (i.e., the boresight direction) of the antenna [2][3].

The sum mode, used both in transmission (i.e., for the generation of the radar pulses aimed at sensing the surrounding environment) and in reception (i.e., for detecting the presence and range of a target through a monopulse comparator), is obtained by summing the signal from the four quadrants in phase. Under the assumption of quadrantal symmetry for the excitations [24], the sum pattern can be expressed as follows

$$\mathcal{S}(\theta,\phi) = 4\sum_{m=1}^{M}\sum_{n=1}^{N}\alpha_{mn}\cos\left(\frac{2m-1}{2}\psi_x\right)\cos\left(\frac{2n-1}{2}\psi_y\right) \tag{1}$$

where α_{mn}, $m = 1, ..., M$, $n = 1, ..., N$, are real excitation weights. Moreover, $\psi_x = kd_x\sin\theta\cos\phi$, $\psi_y = kd_y\sin\theta\sin\phi$, $k = \frac{2\pi}{\lambda}$ is the free-space wavenumber, λ being the wavelength.

The couple of difference mode signals used to determine the azimuthal and elevation OBA are generated summing in phase reversal pairs of quadrants of the optimal excitations β_{mn} that afford a desired difference pattern $\mathcal{D}(\theta,\phi)$. More specifically, the following difference pattern is synthesized

$$\mathcal{D}^{az}(\theta,\phi) = 4j\sum_{m=1}^{M}\sum_{n=1}^{N}\beta_{mn}\sin\left(\frac{2m-1}{2}\psi_x\right)\cos\left(\frac{2n-1}{2}\psi_y\right) \tag{2}$$

to track the target along the azimuthal plane $[\mathcal{D}^{az}(\theta,\phi) = \mathcal{D}(\theta,\phi)]$, while the difference pattern for the elevation mode $[\mathcal{D}^{el}(\theta,\phi) = \mathcal{D}\left(\theta,\phi+\frac{\pi}{2}\right)]$ is given by

$$\mathcal{D}^{el}(\theta,\phi) = 4j\sum_{m=1}^{M}\sum_{n=1}^{N}\beta_{mn}\cos\left(\frac{2m-1}{2}\psi_x\right)\sin\left(\frac{2n-1}{2}\psi_y\right). \tag{3}$$

According to the sub-arraying strategy [4], the excitations of the compromise difference patterns turn out to be

$$b_{m,n} = \alpha_{mn}\sum_{q=1}^{Q}\delta_{c_{mnq}}w_q\,;\; m=1,...,M\,;\; n=1,...,N\,;\; q=1,...,Q \tag{4}$$

where $\mathbf{C} = \{c_{mn};\, m=1,...,M;\, n=1,...,N\}$ with $c_{mn}\in[0,Q]$ and $\mathbf{W} = \{w_q;\, q=1,...,Q\}$ are the degrees of freedom of the problem at hand. They are two sets of integer values that code the element grouping and the weights of the corresponding clusters, respectively. In (4), $\delta_{c_{mnq}}$ is the Kronecker delta function defined as: $\delta_{c_{mnq}} = 1$ if the element belongs to the q-th sub-array (i.e., $c_{mn} = q$) and $\delta_{c_{m,nq}} = 0$, otherwise.

Following the guidelines described in [18], given a set of independent excitations $\mathbf{A} = \{\alpha_{mn};\, m=1,...,M;\, n=1,...,N\}$ affording an optimal sum pattern, the solution of the compromise between sum and difference patterns is obtained by minimizing the following cost function

$$\Psi(\mathbf{C}) = \frac{1}{\Gamma}\sum_{m=1}^{M}\sum_{n=1}^{N}\alpha_{mn}^2\left\{g_{mn} - \sum_{q=1}^{Q}\delta_{c_{mnq}}w_q(\mathbf{C})\right\}^2 \tag{5}$$

where $g_{mn} \triangleq \frac{\beta_{mn}}{\alpha_{mn}}$, $m=1,...,M$, $n=1,...,N$ is the set of *optimal gains* and $\Gamma \leq M\times N$ is the number of radiating/active elements in each quadrant. Equation (5) defines a '*least square*' problem and its solution (i.e., the partition that minimizes the cost function) is a contiguous partition whose As for the the unknown weighting vector $\mathbf{W}$ can be it is analytically computed for each trial sub-array configuration $\mathbf{C}$ as follows

$$w_q(\mathbf{C}) = \frac{\sum_{m=1}^{M}\delta_{c_{mnq}}\alpha_{mn}\beta_{mn}}{\sum_{m=1}^{M}\delta_{c_{mnq}}\alpha_{mn}^2}. \tag{6}$$

since the value minimizing the sum of the square distances in a contiguous subset is the

weighted arithmetic mean of the corresponding g_{mn} values. In order to determine the "optimal" sub-array configurations $\mathbf{C}^{opt}$, Eq. (5) is optimized according to the following procedure:

- *Step 1* - **Contiguous Partition Method (CPM)**. Exploiting the theory in [23] for the definition of contiguous partitions least-square grouping of real-valued quantities, $\mathbf{C}^{opt}$ is obtained by choosing Q subsets of the optimal gains g_{mn} sorted on a line [19]. Towards this end, a list $\mathbf{L}$ of Γ reference parameters is generated setting $l_1 = \min_{m,n}\{g_{mn}\}$ and $l_\Gamma = \max_{m,n}\{g_{mn}\}$. In such a way, the number of admissible sub-array configurations (or *contiguous partitions*) belonging to the so-called essential solution space $\Re^{(ess)}$ [1] amounts to $U^{(ess)} = \begin{pmatrix} \Gamma - 1 \\ Q - 1 \end{pmatrix}$.

- *Step 2* - **Solution Space Representation**. Thanks to the sorted list defined at *Step 1*, the solutions in $\Re^{(ess)}$ are coded into a *Direct Acyclic Graph* (*DAG*) [28]. The graph $\mathcal{G}(\Gamma, Q, \Psi)$ represented in Fig. 2 is characterized by:

  - Q rows each one containing $V = (\Gamma - Q + 1)$ vertexes, V being the maximum number of elements that can be grouped in a sub-array;
  - a maximum depth Γ equal to the number of levels of the *DAG* and to the dimension of the list $\mathbf{L}$ as well as the number of vertexes along each r-th path $\mathbf{P}_r$, $r = 1, ..., U^{(ess)}$ in $\mathcal{G}$;
  - a suitability function Ψ (5) aimed at evaluating the goodness of each path $\mathbf{P}_r$, $r = 1, ..., U^{(ess)}$.

  The levels of the *DAG* map one-to-one the elements in $\mathbf{L}$. A vertex v_{q,l_q}, $q = 1, ..., Q$, $l_q = q, ..., q + V - 1$ is identified by its row index, q, and the depth index, l_q. Moreover, its argument, $\arg\left(v_{q,l_q}\right) = q$, indicates the sub-array membership of each array element of the list $\mathbf{L}$. A path $\mathbf{P}$ of Γ vertexes and $\Gamma - 1$ edges codes a trial solution $\mathbf{C}$. As shown in Fig. 2, e^{+}_{q,l_q} is the edge (if present) connecting the vertexes

[1] Essential with respect to the solution space which can be sampled using standard global optimizers whose dimension is $U = Q^\Gamma$.

v_{q,l_q} and v_{q,l_q+1} on the same row of the DAG, while e^{-}_{q,l_q} is the edge (if admissible) between the vertexes v_{q,l_q} and v_{q+1,l_q} on two different rows of the DAG;

- *Step 3* - **Edge Weighting**. In [22], the ACO was used to explore the DAG for identifying the best sub-array configuration $\mathbf{C}^{opt}$. Since the quantity of pheromone $\tau^{\pm}_{q,l_q}(0)$, $q = 1, ..., Q$, $l_q = q, ..., q + V - 1$ was uniformly set, the edges $e^{\pm}_{q,l_q}(0)$, $q = 1, ..., Q$, $l_q = q, ..., q + V - 1$ have at the initialization the same probability of being explored. Because of the DAG structure and the value of the ratio $\frac{V}{Q}$, such a choice affects in a non-negligible way the ACO-based sampling of the DAG. Indeed, some edges paths have a higher probability of being sampled since the vertexes could belong to a different number of paths. As representative examples, the DAGs of the cases ($\Gamma = 8$, $Q = 3$) and ($\Gamma = 8$, $Q = 6$), both having $U^{(ess)} = 21$, are reported in Fig. $3(a)$ and Fig. $3(b)$, respectively. By sake of clarity, the number of solutions to which edge belongs to is indicated.

  In order A proper edge weighting scheme is here adopted to assure a uniform probability of sampling to each solution/path and to allow an unbiased search a proper edge weighting scheme is necessary. Towards this end, The effect is that of increasing/reducing the level of pheromone on each edge is increased/reduced proportionally to the number of different contiguous partition defined through that edge. Let us observe that the number of paths leaving the root vertex $v_{1,1}$ corresponds to the dimension of the whole solution space $\Omega_{1,1} = U^{(ess)} = \begin{pmatrix} \Gamma - 1 \\ Q - 1 \end{pmatrix}$, while those departing from the vertex $v_{1,2}$ [Fig. $4(a)$] and $v_{2,2}$ [Fig. $4(b)$] are $\Omega_{1,2} = \begin{pmatrix} \Gamma - 2 \\ Q - 1 \end{pmatrix}$ and $\Omega_{2,2} = \begin{pmatrix} \Gamma - 2 \\ Q - 2 \end{pmatrix}$, namely the number of path through $\mathcal{G}(\Gamma - 1, Q, \Psi)$ and $\mathcal{G}(\Gamma - 1, Q - 1, \Psi)$, respectively. Generalizing, the number Ω of paths/solutions

available from the generic vertex v_{q,l_q} is equal to

$$\Omega_{q,l_q} = \begin{pmatrix} \Gamma - l_q \\ Q - q \end{pmatrix}. \tag{7}$$

Therefore, the edge-weighting scheme is applied at the initialization ($j = 0$) as follows: Accordingly, the level of pheromone on edge e^{+}_{q,l_q} is set to

$$\tau^{+}_{q,l_q}(j) = \frac{\Omega_{q,l_q+1}}{\Omega_{q,l_q}} \tag{8}$$

while on the edge e^{-}_{q,l_q}

$$\tau^{-}_{q,l_q}(j) = \frac{\Omega_{q+1,l_q}}{\Omega_{q,l_q}}. \tag{9}$$

It is worth noting that $\Omega_{q,l_q} = \Omega_{q,l_q+1} + \Omega_{q+1,l_q}$.

- *Step 4 - DAG ACO*-**Sampling**. Iteratively, the *ACO* [20][25] explores the *DAG* to find $\mathbf{C}^{opt}$. Each ant of the colony $\mathbf{A}(j) = \{\mathrm{a}_t(j);\, t = 1, ..., T\}$, T being the colony dimension, samples the graph starting from the root $v_{1,1}$ and choosing the next edge with probability

$$\eta^{\pm}_{q,l_q}(j) = \frac{\tau^{\pm}_{q,l_q}(j)}{\tau^{+}_{q,l_q}(j) + \tau^{-}_{q,l_q}(j)},\ q = 1, ..., Q;\ l_q = q, ..., q + V - 1. \tag{10}$$

The set of vertexes visited by an ant, $\mathrm{a}_t(j)$, from the root to the end of the graph codes a path $\mathbf{P}_t(j) = \left\{v_{q,l_q};\, q = 1, ..., Q;\, l_q = 1, ..., \Gamma\right\}$ of Γ vertexes composed by $\Gamma - 1$ edges that identifies a trial sub-array configuration $\mathbf{C}_t(j) = \arg\{\mathbf{P}_t(j)\}$. The optimality of each trial solution is quantified by the value of the cost function in correspondence with the corresponding subarray configuration, $\Psi(\mathbf{C}_t(j))$. Such an information is exploited to update the pheromone level on the edges of the *DAG* as

$$\tau^{\pm}_{q,l_q}(j+1) \leftarrow (1-\rho)\left[\tau^{\pm}_{q,l_q}(j) + \sum_{t=1}^{T} \frac{H \times \Psi_j^{min}}{\Psi(\mathbf{C}_t(j))}\right] \tag{11}$$

where either e^{+}_{q,l_q} or $e^{-}_{q,l_q} \in \mathbf{P}_t(j)$ and $\Psi^{min}_j = \min_{t=1,\dots,T}\{\Psi(\mathbf{C}_t(j))\}$. Moreover, $\rho \in (0,1]$ and H are positive indexes that control the pheromone evaporation and deposition on the edges of the DAG. The algorithm stops when a maximum number of iterations J_{max} is reached or the minimization of the cost function reaches a stationary point ($j = J_{stat}$), then $\mathbf{C}^{opt}$ chosen as

$$\mathbf{C}^{opt} = arg\left[\min_j \min_t \{\Psi(\mathbf{C}_t(j))\}\right]. \tag{12}$$

3 Numerical Results

A set of numerical experiments has been carried out to point out the potentialities of the proposed approach as well as its improvements over previous implementations.

The first example deals with the synthesis of a small array in order to detail in a comparative fashion the behavior of the edge-weighted approach versus the uniform technique [22]. The array elements are located on a regular lattice with $M = N = 3$ ($d_x = d_y = \frac{\lambda}{2}$) and belong to a circular support of radius $R = 1.5\lambda$ such that the resulting arrangement is composed by $\Gamma = 32$ radiators (8 for each quadrant). The excitations of the sum mode (Fig. 5) have been chosen to afford a Taylor pattern with $SLL = -35\,dB$ and $\bar{n} = 6$ [24]. As far as the reference difference beam $\mathcal{D}(\theta,\phi)$ is concerned, a Bayliss pattern with $SLL = -30\,dB$ and $\bar{n} = 7$ [24] has been used by setting the excitation distribution as in Fig. 6.

The compromise difference beam has been synthesized varying the number of sub-arrays in the range $Q \in [2,6]$ to analyze the performance of the proposed method. First, the Γ optimal gains have been computed and the list $\mathbf{L}$ generated (Fig. 7) according to the CPM.

Figure 8 shows the values of the cost function for the best solutions found by the proposed weighted-graph ACO-based ($WG-ACO$) approach and the ACO version in [22] when running 10 different simulations for each value of Q. The ACO parameters have been set

according to the outcomes from [22]: $T = 0.1 \times U^{(ess)}$ with a minimum value equal to $T_{min} = 5$ to exploit the cooperative behavior of the colony, $J_{max} = 1000$, $H = 1$, and $\rho = 0.05$. It is worth noting that both methods find the global optimum when Q is smaller than Γ (e.g., $Q = \{2, 3, 4\}$) as confirmed by the plot in Fig. $9(a)$ that shows the cost function values for all the solutions belonging to $\Re^{(ess)}$ ($\Gamma = 8$, $Q = \{2, 3, 4\}$). Nevertheless, the bare ACO does not reach the global solution when $Q \simeq \Gamma$ ($\Gamma = 8$, $Q = \{5, 6\}$) since it gets stuck in a local minimum [Fig. $9(b)$]. As a matter of fact, $\Psi^{opt}_{WG-ACO}\big|_{Q=5} = 5.023{\times}10^{-4}$ vs. $\Psi^{opt}_{ACO}\big|_{Q=5} = 5.438{\times}10^{-4}$ and $\Psi^{opt}_{WG-ACO}\big|_{Q=6} = 1.685{\times}10^{-4}$ vs. $\Psi^{opt}_{ACO}\big|_{Q=6} = 4.965{\times}10^{-4}$. The corresponding paths within the DAG are as follows: $\underline{P}^{opt}_{WG-ACO}\big|_{Q=5} = \{11123445\}$ vs. $\underline{P}^{opt}_{ACO}\big|_{Q=5} = \{12234445\}$ and $\underline{P}^{opt}_{WG-ACO}\big|_{Q=6} = \{12234556\}$ vs. $\underline{P}^{opt}_{ACO}\big|_{Q=6} = \{11123456\}$. Let us notice that, despite the dimension of the solution space does not vary from $Q = 3$ up to $Q = 6$ (see Tab. I), the uniform ACO is able to get the "best" compromise solution only in the former case, while sub-optimal solutions are found otherwise. Such a result is not due to the DAG representation of the solution space, but on the "control level" of the ACO [25] (i.e., control parameters, initialization criteria, constraints, and termination conditions) which exploits the *pheromone update mechanism* to sample the solution space looking for the global optimum. As a matter of fact, still keeping the same ACO structure presented in [22], but initializing the pheromone levels through the weighted approach, the reliability of the DAG sampling has been improved. As an illustrative example, Figure 10 gives a representation of the relative amount of pheromone on the edges of the DAG for the case ($\Gamma = 8$, $Q = 3$) [Fig. $10(a)$] and the case ($\Gamma = 8$, $Q = 6$) [Fig. $10(b)$]. More in detail, the thickness of the segments between two vertexes is proportional to the amount of pheromone on the corresponding edge. Moreover, the dotted lines indicate obliged choices when only the corresponding path is admissible.

The inefficiencies of the uniform-weight approach is more evident when $U^{(ess)}$ grows as pointed out by the plots of Ψ^{opt} in Fig. 11. The test case is here concerned with a lattice of dimension $2M \times 2N = 20 \times 20$, a circular boundary $R = 5.0\lambda$ in radius, and a number of active elements for each quadrant equal to $\Gamma = 75$. The number of sub-arrays has been varied between $Q = 2$ and $Q = 20$. As for the excitations, the sum excitations was chosen

to afford a Taylor pattern with $SLL = -35\,dB$ and $\bar{n} = 6$ [24], while reference excitations was used to generate a Bayliss pattern with $SLL = -30\,dB$ and $\bar{n} = 7$ [24]. Concerning the parameters of the ACO, the same setting of the previous experiment has been used also introducing a maximum threshold $T_{max} = 1000$ (when $T = 0.1 \times U^{(ess)} > T_{max}$) on the number of ants for each iteration to limit the computational time. As expected (Fig. 11), the weighted approach always outperforms the previous implementation and, for each example (i.e., U^{ess} value or Q value), solutions with lower cost function values have been determined.

As far as the computational issues are concerned, let us consider that the CPU-time required to complete an ACO iteration is the same for both the weighted and uniform scheme. It is also worth noticing that the improvements from the weighted scheme are not concerned with the convergence speed, but rely in a more reliable search of the optimal solution. For completeness and as a representative example, the case $Q = 5$ needs $J_{stat} = 85$ iterations of the $WG - ACO$ (i.e., a total CPU-time of 16.34 sec) to sample the solution space of dimension $U^{(ess)} = 1150626$, while the uniform approach with the same ACO parameter setting stops after $J_{stat} = 122$ iterations (i.e., a total CPU-time of 23.28 sec).

3.1 The Hybrid Extension

Although the $WG - ACO$ proved its effectiveness, the computation of the sub-array weights through (6) does not guarantee the retrieval of the global optimum solution. Moreover, it does not allow to set constraints on the desired radiation pattern in a direct fashion [26][27]. The hybrid method in [11][29] overcomes such a limitation. Once $\mathbf{C}^{opt}$ was defined by means of the $WG - ACO$, the optimal weights $\mathbf{W}^{opt}$ can be computed by means of a convex programming (CP) strategy [30], aimed at minimizing

$$\Phi(\mathbf{W}) = -\mathrm{Im}\left\{\frac{\partial \mathcal{D}(\theta,\phi)}{\partial \gamma}\right\}_{\gamma=\{\theta,\phi\}}\Bigg|_{\substack{\theta=\theta_0 \\ \phi=\phi_0}} \tag{13}$$

to the maximize the slope along the boresight direction (θ_0, ϕ_0) of the difference pattern $\mathcal{D}(\theta, \phi)$, subject to $\mathrm{Re}\left\{\frac{\partial \mathcal{D}(\theta,\phi)}{\partial \gamma}\right\}_{\gamma=\{\theta,\phi\}}\Big|_{\substack{\theta=\theta_0 \\ \phi=\phi_0}} = 0$, $\mathcal{D}(\theta_0, \phi_0) = 0$, and $|\mathcal{D}(\theta, \phi)|^2 \leq \mathcal{M}(\theta, \phi)$, $\mathcal{M}(\theta, \phi)$ being a positive upper bound function on the power radiated in the sidelobe region. Moreover, $\mathrm{Re}\{\,\}$ and $\mathrm{Im}\{\,\}$ indicate the real and imaginary part, respectively. Furthermore, $\theta \in \left[0, \frac{\pi}{2}\right]$ and $\phi \in [0, 2\pi]$.

To show the behavior of the hybrid method $(H-WG-ACO)$, an array with $M = N = 5$ elements located on a square grid with uniform spacing $d = \frac{\lambda}{2}$ is used as benchmark geometry. The aperture radius has been set to $R = 2.5\lambda$ such that $\Gamma = 19$. The same sum pattern of the previous examples has been kept, while the reference difference excitations β_{mn} [Figs. $12(a)$-(b)] have been generated by applying the procedure in [30] to synthesize the optimal difference pattern $D(\theta, \phi)$ with $SLL^{ref} = -25\,dB$ shown in Fig. $12(c)$. In order to design the compromise difference pattern, $Q = 5$ sub-arrays have been used for each quadrant.

The array clustering found by the $WG - ACO$ when exploring the solution graph with $T = 30$ ants is shown in Fig. $13(a)$. Successively, the convex programming procedure has been applied by constraining the pattern to the same mask used to determine the optimal difference pattern [Fig. $12(c)$]. The values $\mathbf{W}^{opt}$ are then given in Tab. II, while the corresponding pattern is shown in Fig. $13(b)$. For comparison, the same synthesis problem has been addressed with the hybrid-BEM $(H - BEM)$ approach [19] and the results are reported in Fig. 13 and Tab. II, as well. For completeness, Figure 14 plots the level of the secondary lobe normalized to the maximum of the power pattern for each ϕ-cut, $\phi \in [0 : 80^o]$ [Fig. $14(a)$] and the sidelobe ratio defined as $SLR(\phi) = \frac{SLL(\phi)}{max_{0\leq\theta<\frac{\pi}{2}}[\mathcal{D}(\theta,\phi)]}$, $\phi \in [0 : 80^o]$ [Fig. $14(b)$]. As it can be observed, the $H - WG - ACO$ solution improves that obtained with the $H - BEM$ in terms of maximum SLL ($SLL_{H-BEM} = -21.3\,dB$ vs. $SLL_{H-WG-ACO} = -25.4\,dB$) and SLR value, which turns out to be smaller in a large part (i.e., almost 90%) of the angular range. The reliability of the new hybridization in better matching the reference pattern $\mathcal{D}(\theta, \phi)$ [Fig. $12(c)$] is further pointed out in Fig. 15 where the mismatch index $\Xi(\theta, \phi) \triangleq \left|\mathcal{D}_{dB}(\theta, \phi) - \mathcal{D}^{H}_{dB}(\theta, \phi)\right|$ is shown for both hybrid

methods.

Finally, in order to give some indications on the computational costs of the hybrid ACO-based approach, let us consider that sampling the solution space of dimension $U^{(ess)} = 3060$ requires 133 ACO iterations and 11CP iterations when using the $H - WG - ACO$ [i.e., 5.8×10^{-2}sec $(WG - AGO)$ and 850 sec (CP)], while the $H - BEM$ performs 22 BEM iterations and 17 CP iterations [i.e., $< 10^{-6}$ sec (BEM) and 1370 sec (CP)].

4 Conclusions

In this work, an edge weighting technique has been proposed for the effective ACO-based sampling of the graph architecture coding the admissible clustering configurations of a sub-arrayed monopulse planar array. The advantages of the ACO in dealing with the non-convexity of the problem at hand and to explore graph representations of the solution space have been further and better exploited for enabling the synthesis of large-scale planar arrangements. Representative results have demonstrated the enhancement of the synthesis performance with respect to previous methods (e.g., BEM) and implementations (i.e., uniform ACO).

References

[1] M. I. Skolnik, *Radar Handbook* (3rd Edition). USA: McGraw-Hill, 2008.

[2] S. M. Sherman, *Monopulse Principles and Techniques*. USA: Artech House, 1984.

[3] D. K. Barton, *Monopulse Radar*. USA: Artech House, 1977.

[4] D. A. McNamara, "Synthesis of sub-arrayed monopulse linear arrays through matching of independently optimum sum and difference excitations," *IEE Proc. H Microwaves Antennas Propag.*, vol. 135, no. 5, pp. 371-374, Oct. 1988.

[5] T.-S. Lee and T.-Y. Dai, "Optimum beamformers for monopulse angle estimation using overlapping subarrays," *IEEE Trans. Antennas Propag.*, vol. 42, no. 5, pp. 651-657, May 1994.

[6] T.-S. Lee and T.-K. Tseng, "Subarray-synthesized low-side-lobe sum and difference patterns with partial common weights," *IEEE Trans. Antennas Propag.*, vol. 41, no. 6, pp. 791-800, Jun. 1993.

[7] A. F. Morabito and P. Rocca, "Optimal synthesis of sum and difference patterns with arbitrary sidelobes subject to common excitations constraints," *IEEE Antennas Wireless Propag. Lett.*, vol. 9, pp. 623-626, 2010.

[8] F. Ares, S. R. Rengarajan, J. A. Rodriguez, and E. Moreno, "Optimal compromise among sum and difference patterns," *J. Electromag. Waves Appl.*, vol. 10, pp. 1143-1555, 1996.

[9] P. Lopez, J. A. Rodriguez, F. Ares, and E. Moreno, "Subarray weighting for difference patterns of monopulse antennas: Joint optimization of subarray configurations and weights," *IEEE Trans. Antennas Propag.*, vol. 49, no. 11, pp. 1606-1608, Nov. 2001.

[10] S. Caorsi, A. Massa, M. Pastorino, and A. Randazzo, "Optimization of the difference patterns for monopulse antennas by a hybrid real/integer-coded differential evolution method," *IEEE Trans. Antennas Propag.*, vol. 53, no. 1, pp. 372-376, Jan. 2005.

[11] M. D'Urso, T. Isernia, and E. F. Meliado', "An effective hybrid approach for the optimal synthesis of monopulse antennas," *IEEE Trans. Antennas Propag.*, vol. 55, no. 4, pp. 1059-1066, Apr. 2007.

[12] P. Rocca, L. Manica, A. Martini, and A. Massa, "Synthesis of large monopulse linear arrays through a tree-based optimal excitations matching," *IEEE Antennas Wireless Propag. Lett.*, vol. 6, pp. 436-439, 2007.

[13] Y. Chen, S. Yang, and Z. Nie, "The application of a modified differential evolution strategy to some array pattern synthesis problems," *IEEE Trans. Antennas Propag.*, vol. 56, no. 7, pp. 1919-1927, Jul. 2008.

[14] L. Manica, P. Rocca, and A. Massa, "On the synthesis of sub-arrayed planar array antennas for tracking radar applications," *IEEE Antennas Wireless Propag. Lett.*, vol. 7, pp. 599-602, 2008.

[15] L. Manica, P. Rocca, and A. Massa, "An excitation matching procedure for sub-arrayed monopulse arrays with maximum directivity," *IET Radar, Sonar & Navigation*, vol. 3, no. 1, pp. 42-48, Feb. 2009.

[16] P. Rocca, L. Manica, and A. Massa, "Directivity optimization in planar sub-arrayed monopulse antenna," *PIER L*, vol. 4, pp. 1-7, 2008.

[17] P. Rocca, L. Manica, M. Pastorino, and A. Massa, "Boresight slope optimization of sub-arrayed linear arrays through the contiguous partition method," *IEEE Antennas Wireless Propagat. Lett.*, vol. 8, pp. 253- 257, 2008.

[18] L. Manica, P. Rocca, A. Martini, and A. Massa, "An innovative approach based on a tree-searching algorithm for the optimal matching of independently optimum sum and difference excitations," *IEEE Trans. Antennas Propag.*, vol. 56, no. 1, pp. 58-66, Jan. 2008.

[19] L. Manica, P. Rocca, M. Benedetti, and A. Massa, "A fast graph-searching algorithm enabling the efficient synthesis of sub-arrayed planar monopulse antennas," *IEEE Trans. Antennas Propag.*, vol. 57, no. 3, pp. 652-663, Mar. 2009.

[20] M. Dorigo, V. Maniezzo, and A. Colorni, "Ant system: optimization by a colony of cooperating agents," *IEEE Trans. Syst. Man and Cybern. B* , vol. 26, no. 1, pp. 29-41, Feb. 1996.

[21] P. Rocca, L. Manica, F. Stringari, and A. Massa, "Ant colony optimization for tree-searching based synthesis of monopulse array antenna," *Electron. Lett.*, vol. 44, no. 13, pp.783-785, Jun. 2008.

[22] P. Rocca, L. Manica, and A. Massa, "An improved excitation matching method based on an ant colony optimization for suboptimal-free clustering in sum-difference compromise synthesis," *IEEE Trans. Antennas Propag.*, vol. 57, no. 8, pp. 2297-2306, Aug. 2009.

[23] W. D. Fisher, "On grouping of maximum homogeneity," *American Statistical Journal*, pp. 789-798, Dec. 1958.

[24] R. S. Elliott, *Antenna Theory and Design*. Wiley-Interscience IEEE Press, 2003.

[25] P. Rocca, M. Benedetti, M. Donelli, D. Franceschini, and A. Massa, "Evolutionary Optimization as Applied to Inverse Scattering Problems," *Inverse Problems*, vol. 25, p. 1-41, 2009.

[26] P. Rocca, L. Manica, and A. Massa, "Synthesis of monopulse antennas through the iterative contiguous partition method," *Electron. Lett.*, vol. 43, no. 16, pp. 854-856, Aug. 2007.

[27] P. Rocca, L. Manica, A. Martini, and A. Massa, "Compromise sum-difference optimization through the iterative contiguous partition method," *IET Microwaves, Antennas & Propagat.*, vol. 3, no. 2, pp. 348-361, 2009.

[28] P. Rocca, L. Manica, and A. Massa, "An effective matching method for the synthesis of optimal compromise between sum and difference patterns in planar arrays," *PIER B*, vol. 3, pp. 115-130, 2008.

[29] P. Rocca, L. Manica, R. Azaro, and A. Massa, "A hybrid approach for the synthesis of sub-arrayed monopulse linear arrays," *IEEE Trans. Antennas Propagat.*, vol. 57, no. 1, pp. 280-283, Jan. 2009.

[30] O. Bucci, M. D'Urso, and T. Isernia, "Optimal synthesis of difference patterns subject to arbitrary sidelobe bounds by using arbitrary array antennas," *IEE Proc. Microwaves Antennas Propag.*, vol. 152, no. 3, pp. 129-137, Jun. 2005.

FIGURE CAPTIONS

- **Figure 1.** Sketch of a sub-arrayed monopulse array antenna.
- **Figure 2.** *DAG* representation of the solution space.
- **Figure 3.** *DAG Analysis* ($\Gamma = 8$, $Q = \{3, 6\}$) - Number of trial solutions to which the *DAG* edges belong to when (a) $\Gamma = 8$, $Q = 3$ and (b) $\Gamma = 8$, $Q = 6$.
- **Figure 4.** *Edge Weighting Approach* - *DAG* regions admissible from (a) the vertex $v_{1,1}$ and (b) the vertex $v_{2,2}$.
- **Figure 5.** *$WG - ACO$ Numerical Results* ($M = N = 3$, $\Gamma = 8$, $Q \in [2, 6]$) - Excitations of the optimal sum pattern (*Taylor*, $SLL = -35\,dB$, $\bar{n} = 6$ [24]).
- **Figure 6.** *$WG - ACO$ Numerical Results* ($M = N = 3$, $\Gamma = 8$, $Q \in [2, 6]$) - Excitations of the reference difference pattern (*Bayliss*, $SLL^{ref} = -30\,dB$, $\bar{n} = 7$ [24]): (a) amplitudes and (b) phase weights.
- **Figure 7.** *$WG - ACO$ Numerical Results* ($M = N = 3$, $\Gamma = 8$, *Taylor* - $SLL = -35\,dB$ - $\bar{n} = 6$, *Bayliss* - $SLL^{ref} = -30\,dB$ - $\bar{n} = 7$) - List $\mathbf{L}$ of the sorted optimal gains.
- **Figure 8.** *Comparative Assessment* ($M = N = 3$, $\Gamma = 8$, $Q \in [2, 6]$, *Taylor* - $SLL = -35\,dB$ - $\bar{n} = 6$, *Bayliss* - $SLL^{ref} = -30\,dB$ - $\bar{n} = 7$) - Cost function values in correspondence with the optimal solutions found by the *ACO* and the *$WG - ACO$*.
- **Figure 9.** *Comparative Assessment* ($M = N = 3$, $\Gamma = 8$, $Q \in [2, 6]$, *Taylor* - $SLL = -35\,dB$ - $\bar{n} = 6$, *Bayliss* - $SLL^{ref} = -30\,dB$ - $\bar{n} = 7$) - Cost function values of the solutions coded within the *DAG* when (a) $Q \in [2, 5]$ and (b) $Q = \{5, 6\}$. The *ACO* and the *$WG - ACO$* solution are denoted by with a circle.
- **Figure 10.** *$WG - ACO$ Numerical Results* ($\Gamma = 8$, $Q = \{3, 6\}$) - Edge weighting approach as applied to the *DAG* sampling when (a) $\Gamma = 8$, $Q = 3$ and (b) $\Gamma = 8$, $Q = 6$. The dotted lines indicates mandatory choices.

- **Figure 11.** *Comparative Assessment* ($M = N = 20$, $\Gamma = 75$, $Q \in [2, 20]$, *Taylor* - $SLL = -35\,dB$ - $\bar{n} = 6$, *Bayliss* - $SLL^{ref} = -30\,dB$ $\bar{n} = 7$) - Cost function values in correspondence with the optimal solutions found by the ACO and the $WG - ACO$ versus (a) the dimension of the solution space, $U^{(ess)}$, and (b) the number of sub-arrays, Q.

- **Figure 12.** *Hybrid Extension* ($M = N = 5$, $\Gamma = 19$, *Reference difference* [30] - $SLL^{ref} = -25\,dB$) - Reference difference excitations: (a) amplitudes and (b) phase weights. Power pattern of the reference mode (c).

- **Figure 13.** *Hybrid Extension* ($M = N = 5$, $\Gamma = 19$, *Reference difference* [30] - $SLL^{ref} = -25\,dB$, $Q = 5$) - Plots of $(a)(c)$ the sub-array configurations and of $(b)(d)$ the relative power pattern determined with $(a)(b)$ the $H - WG - ACO$ and $(c)(d)$ the $H - BEM$.

- **Figure 14.** *Hybrid Extension* ($M = N = 5$, $\Gamma = 19$, *Reference difference* [30] - $SLL^{ref} = -25\,dB$, $Q = 5$) - Plots of (a) the SLL and (b) the SLR of the solutions found by the $H - WG - ACO$ and the $H - BEM$.

- **Figure 15.** *Hybrid Extension* ($M = N = 5$, $\Gamma = 19$, *Reference difference* [30] - $SLL^{ref} = -25\,dB$, $Q = 5$) - Plot of the mismatch function $\Xi(\theta, \phi)$ when applying the (a) $H - WG - ACO$ and the (b) $H - BEM$.

TABLE CAPTIONS

- **Table I.** $WG - ACO$ *Numerical Results* ($M = N = 3$, $\Gamma = 8$, $Q \in [2, 6]$) - Dimension of the solution space $U^{(ess)}$.

- **Table II.** *Hybrid Approach* ($M = N = 5$, $\Gamma = 19 \times 4$, $Q = 5$) - Values of the sub-array weights.

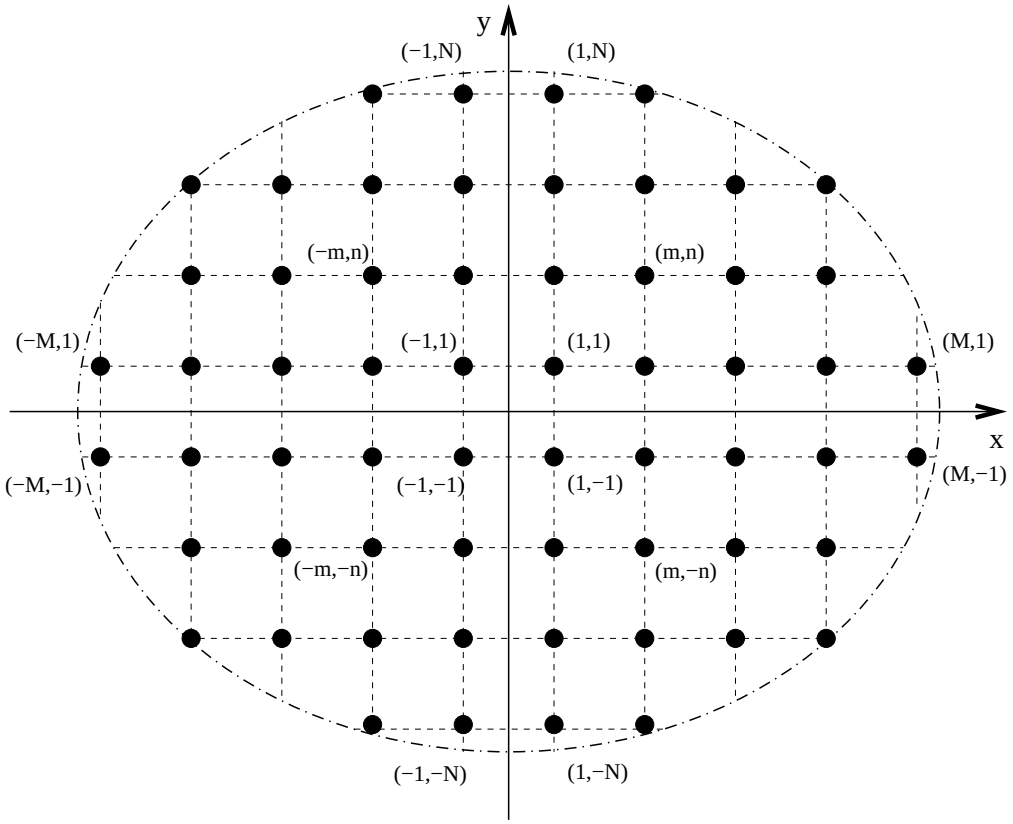

Fig. 1 - G. Oliveri and L. Poli, "Optimal Sub-Arraying of Compromise Planar ..."

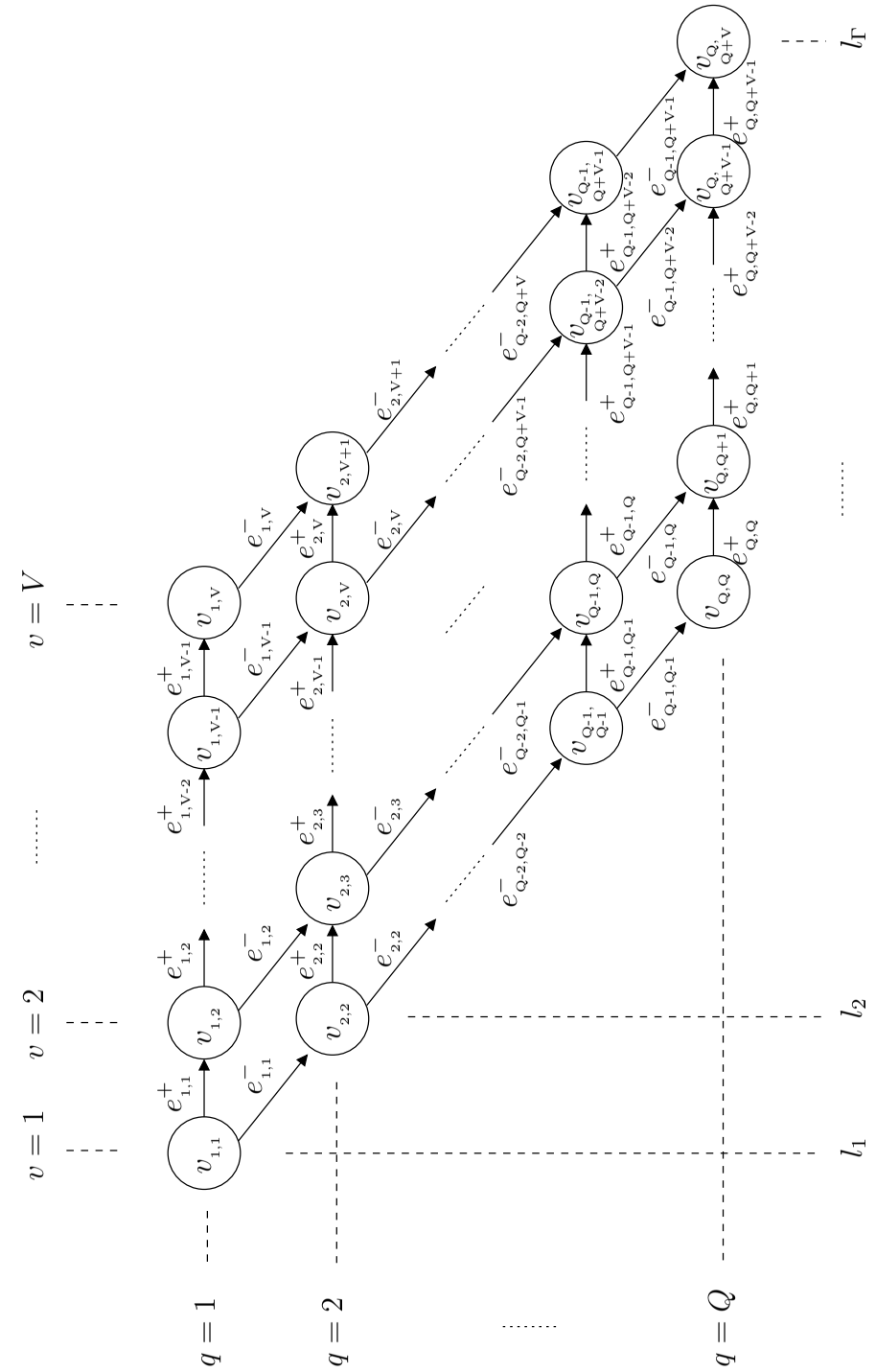

Fig. 2 - G. Oliveri and L. Poli, "Optimal Sub-Arraying of Compromise Planar ..."

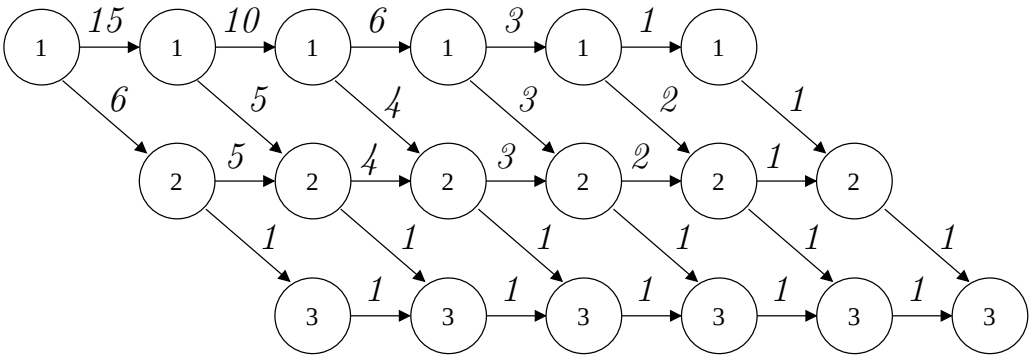

(*a*)

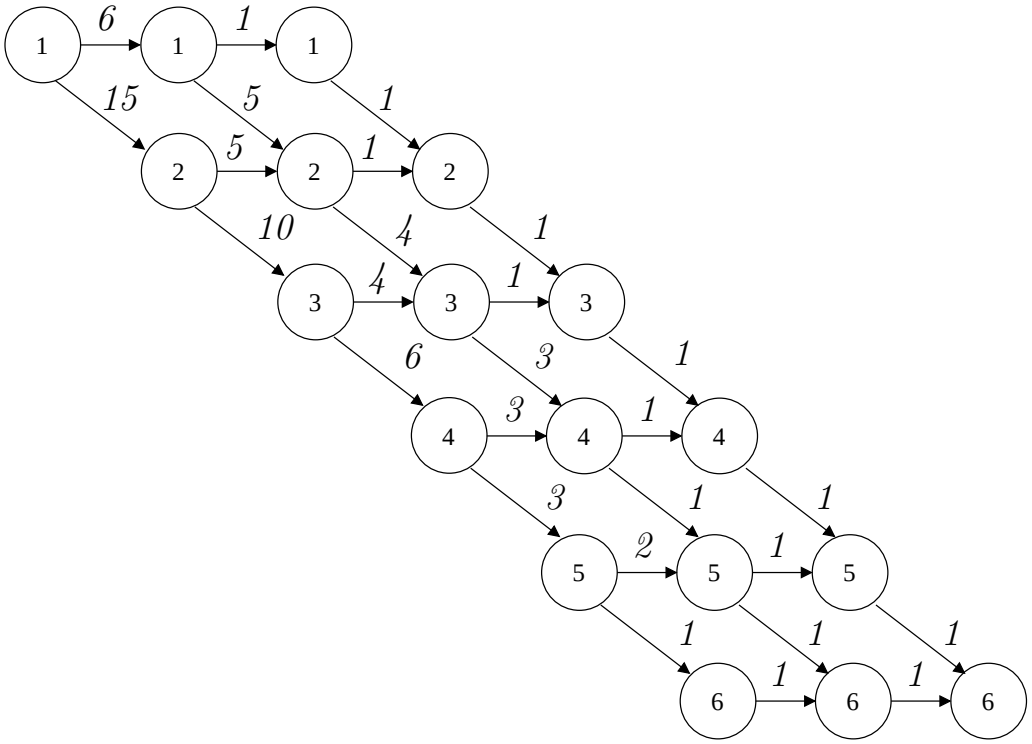

(*b*)

Fig. 3 - G. Oliveri and L. Poli, "Optimal Sub-Arraying of Compromise Planar ..."

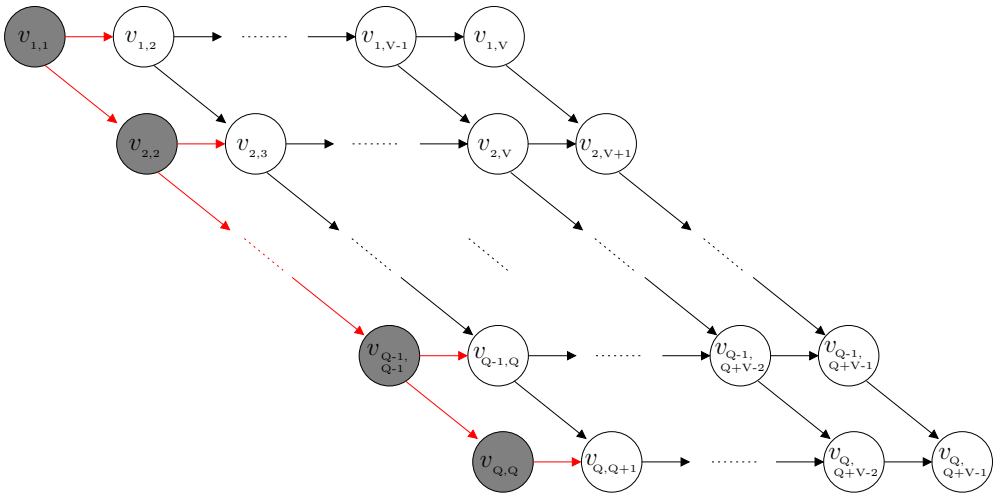

(a)

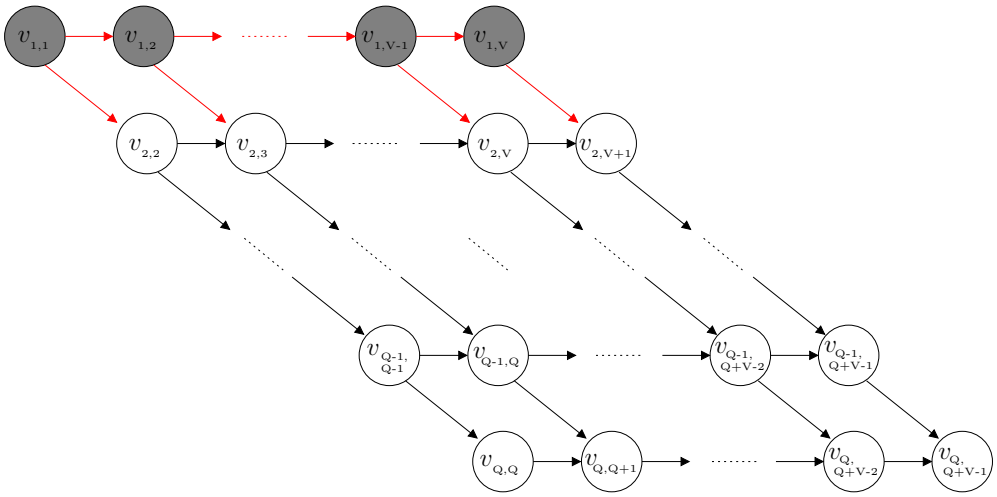

(b)

Fig. 4 - G. Oliveri and L. Poli, "Optimal Sub-Arraying of Compromise Planar ..."

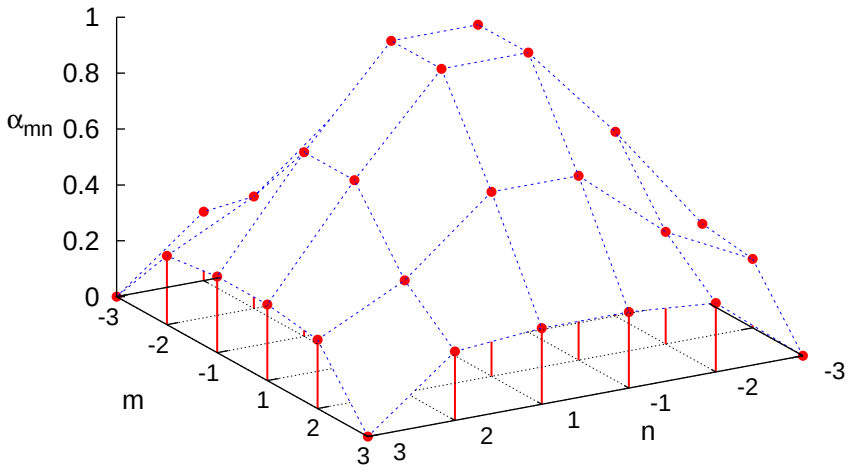

Fig. 5 - G. Oliveri and L. Poli, "Optimal Sub-Arraying of Compromise Planar ..."

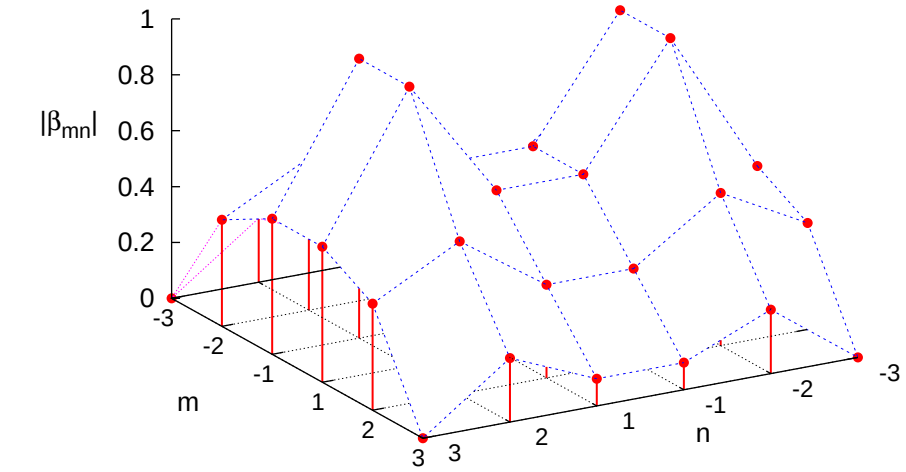

(*a*)

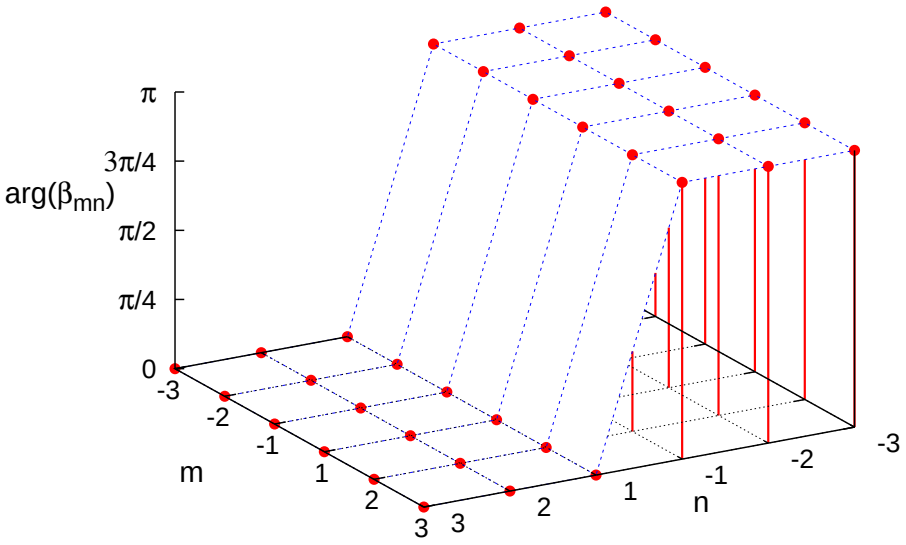

(*b*)

Fig. 6 - G. Oliveri and L. Poli, "Optimal Sub-Arraying of Compromise Planar ..."

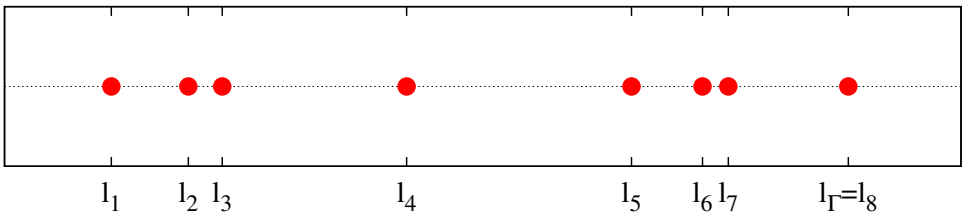

Fig. 7 - G. Oliveri and L. Poli, "Optimal Sub-Arraying of Compromise Planar ..."

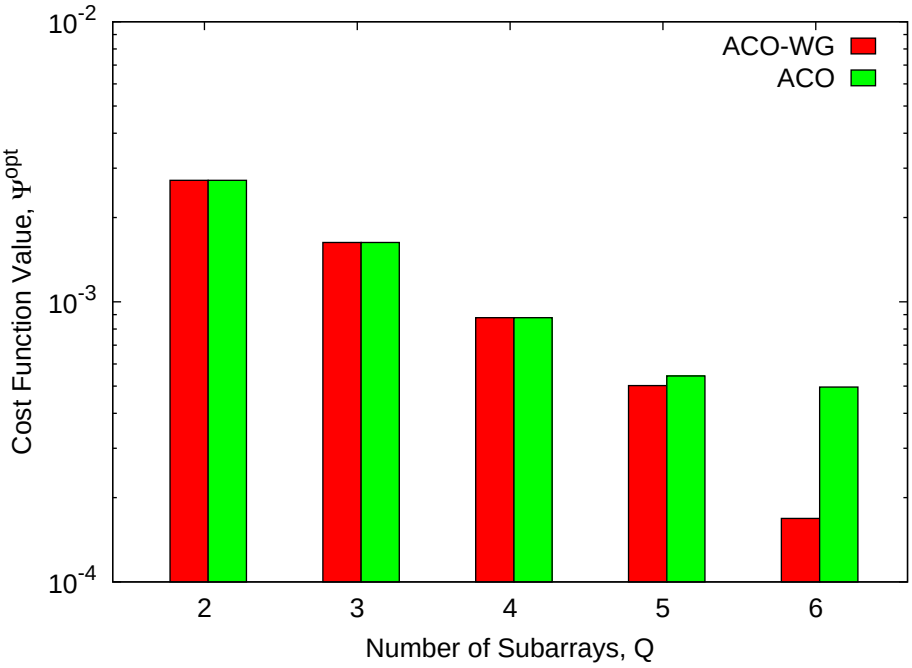

Fig. 8 - G. Oliveri and L. Poli, "Optimal Sub-Arraying of Compromise Planar ..."

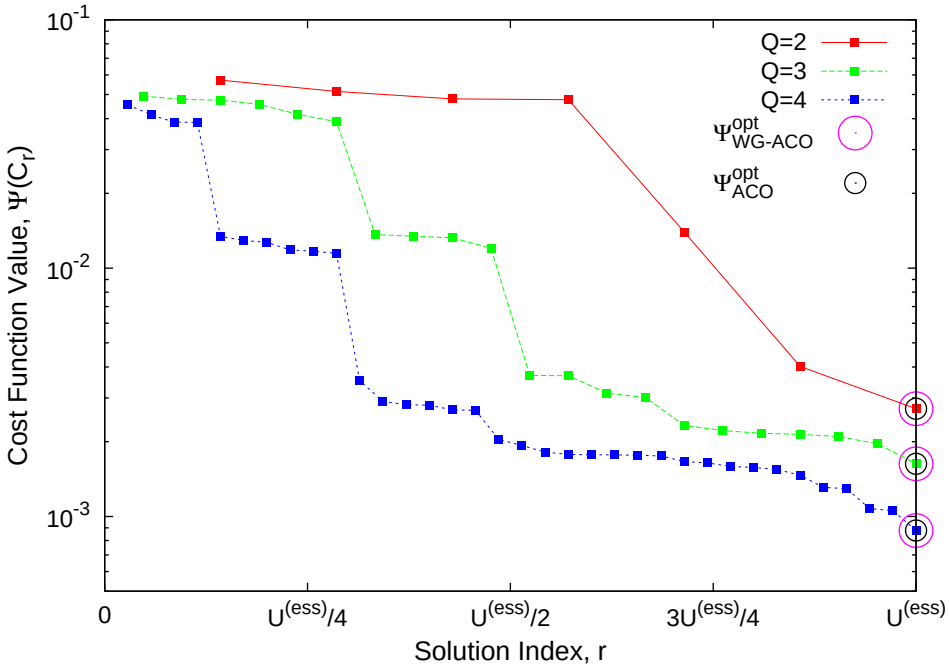

(a)

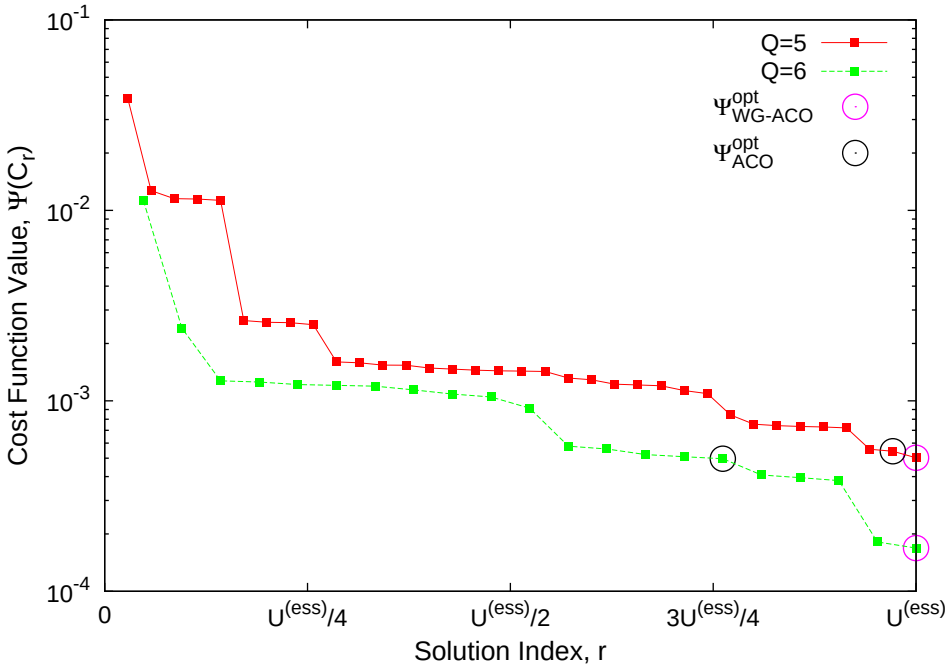

(b)

Fig. 9 - G. Oliveri and L. Poli, "Optimal Sub-Arraying of Compromise Planar ..."

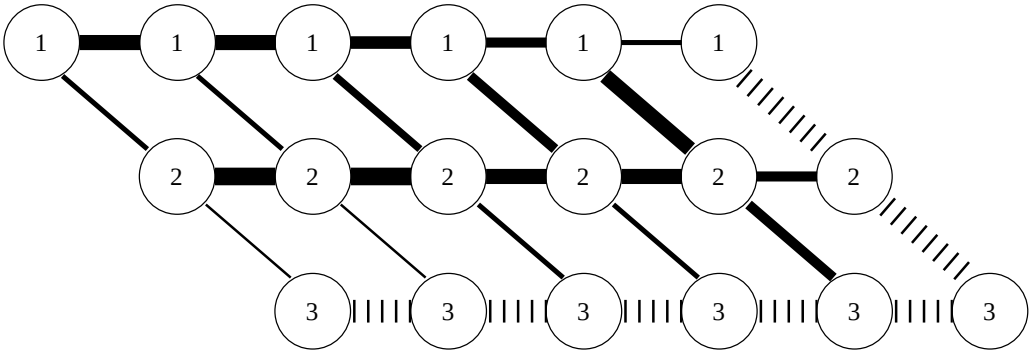

(a)

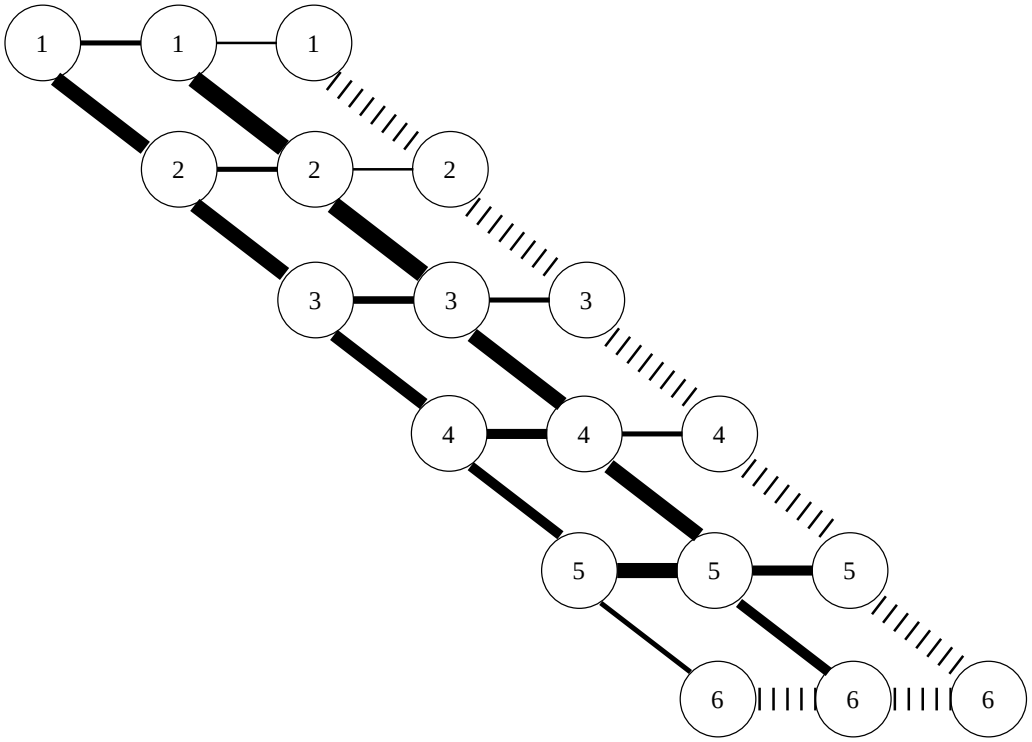

(b)

Fig. 10 - G. Oliveri and L. Poli, "Optimal Sub-Arraying of Compromise Planar ..."

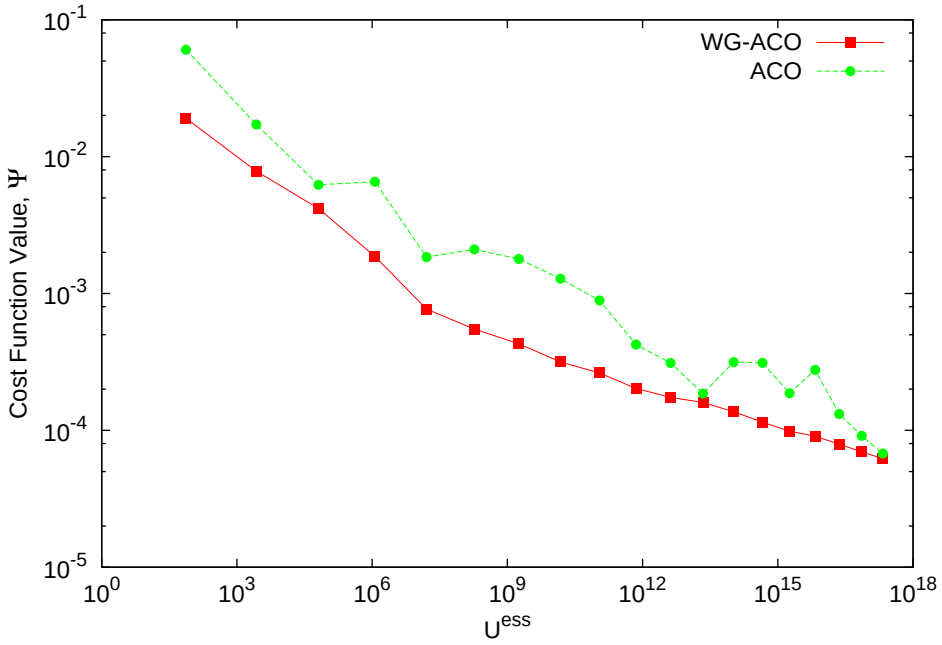

(a)

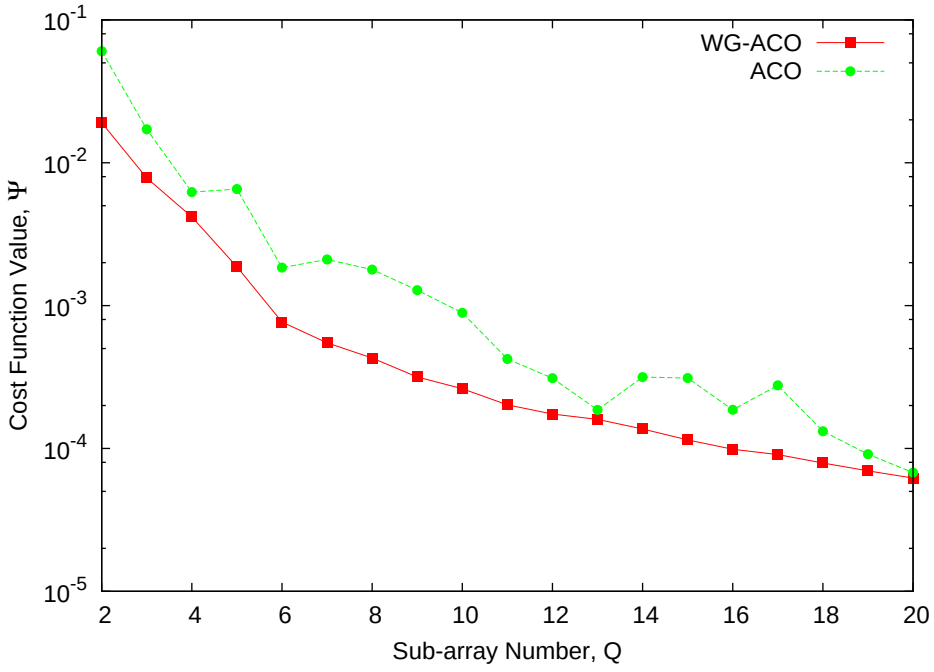

(b)

Fig. 11 - G. Oliveri and L. Poli, "Optimal Sub-Arraying of Compromise Planar ..."

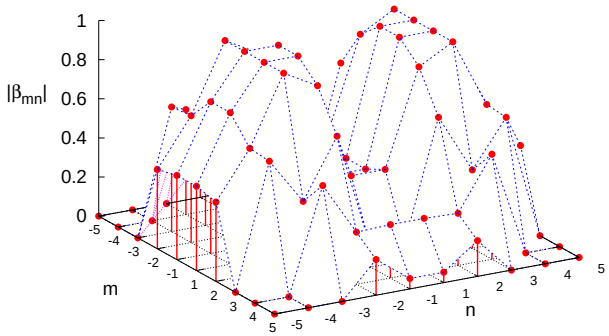

(a)

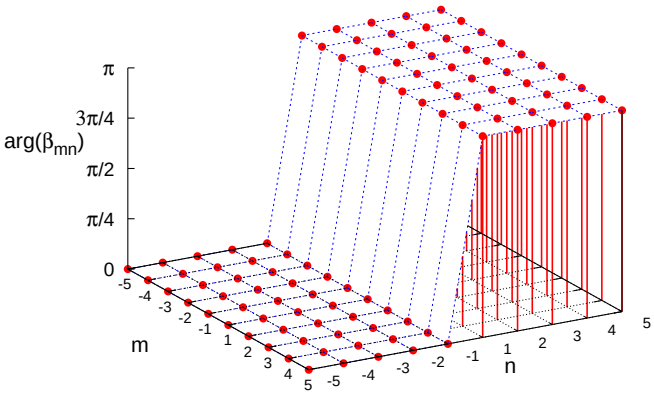

(b)

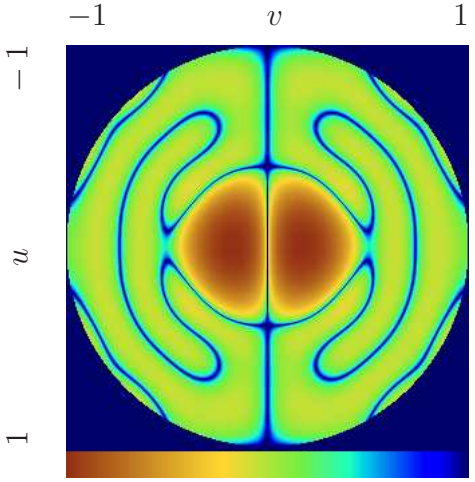

(c)

Fig. 12 - G. Oliveri and L. Poli, "Optimal Sub-Arraying of Compromise Planar ..."

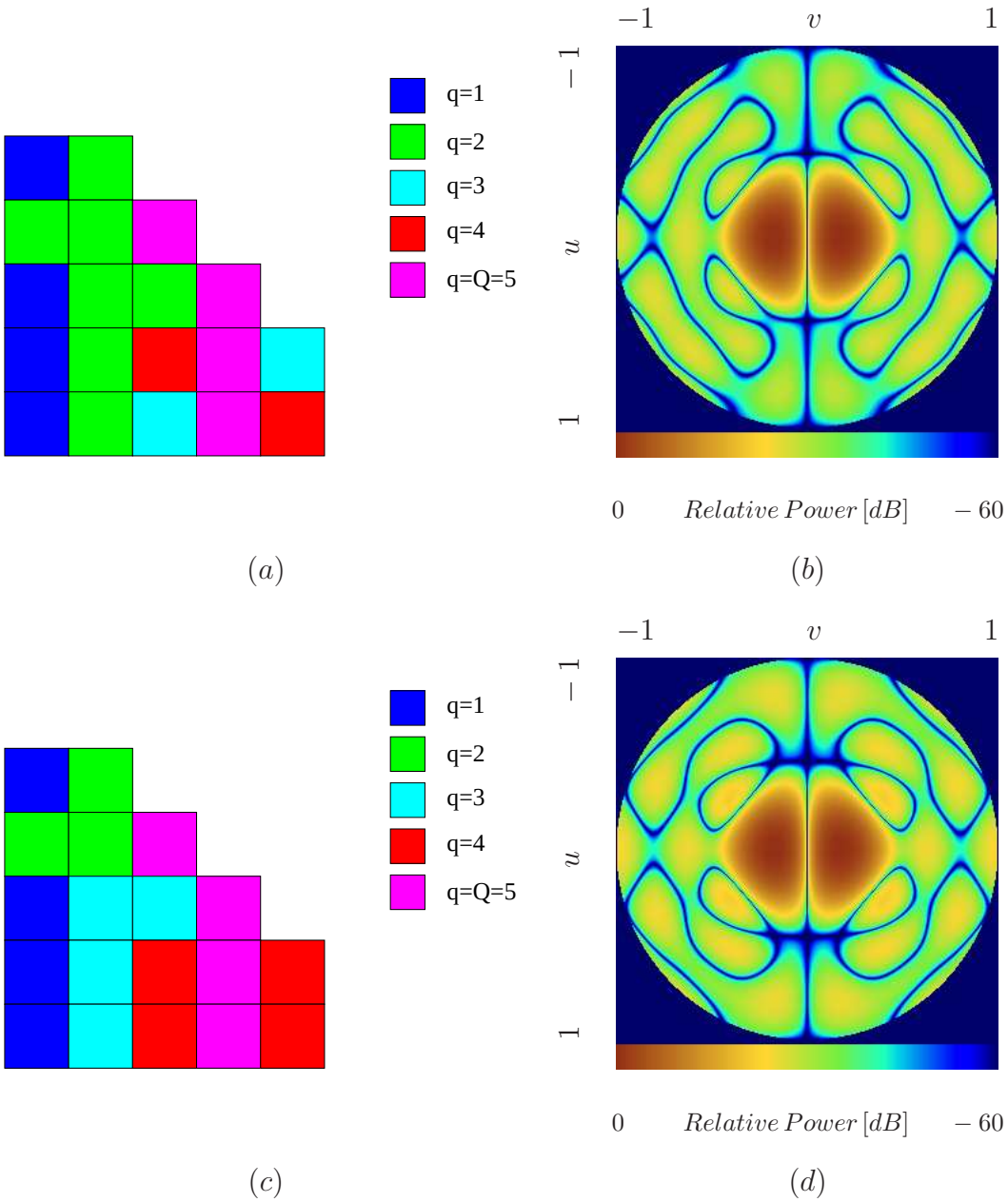

Fig. 13 - G. Oliveri and L. Poli, "Optimal Sub-Arraying of Compromise Planar ..."

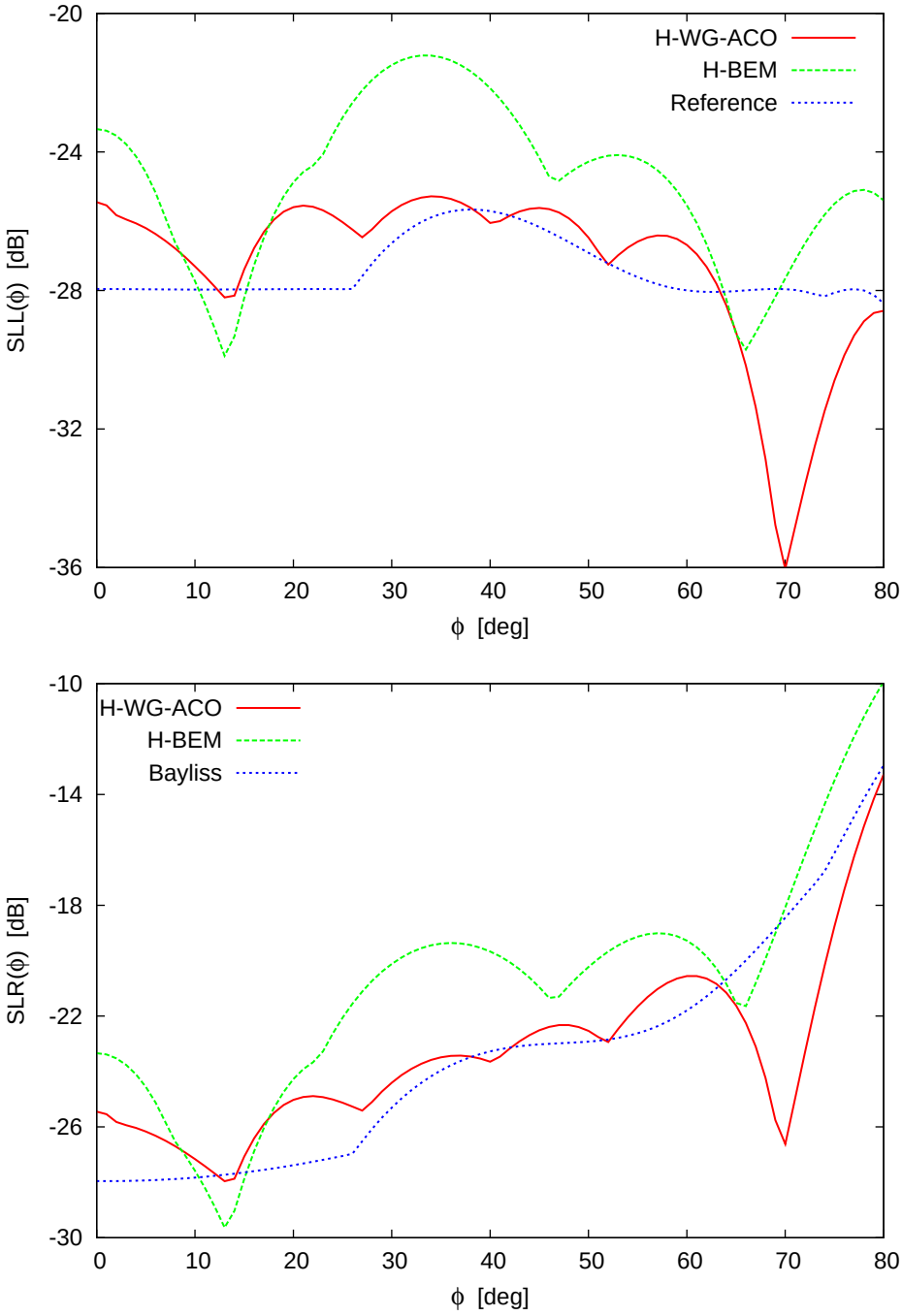

Fig. 14 - G. Oliveri and L. Poli, "Optimal Sub-Arraying of Compromise Planar ..."

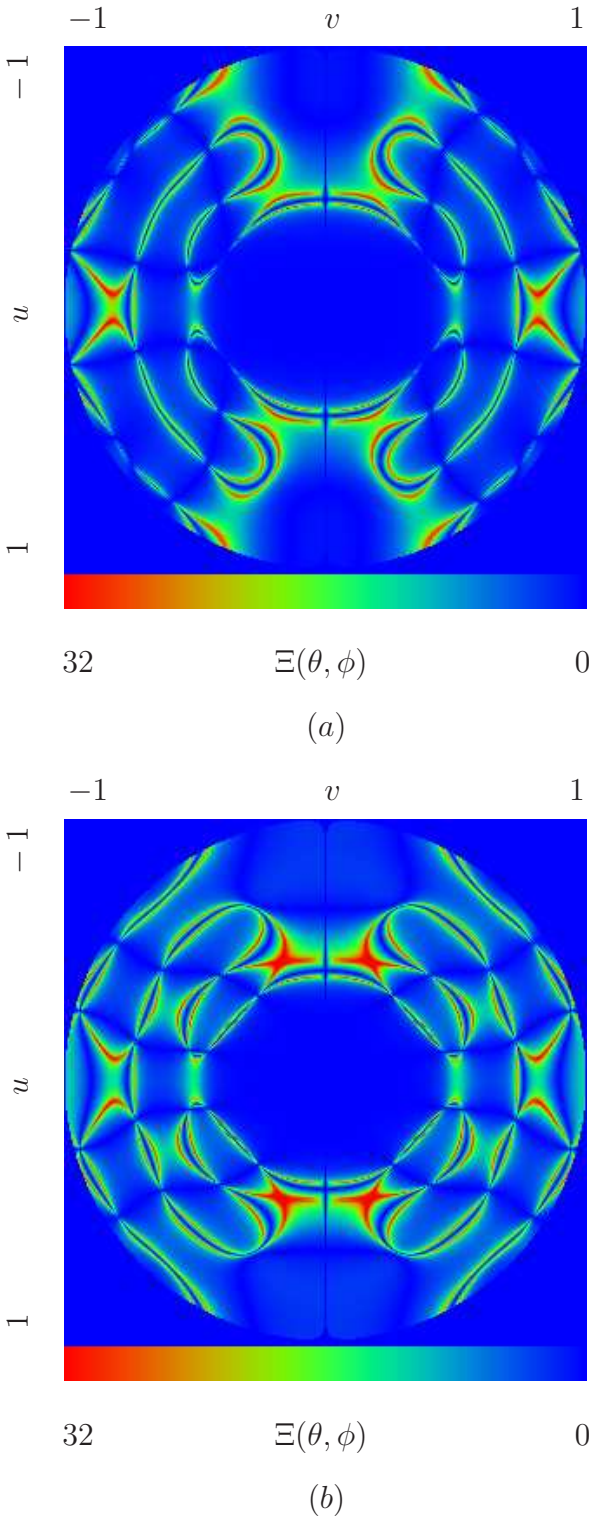

Fig. 15 - G. Oliveri and L. Poli, "Optimal Sub-Arraying of Compromise Planar ..."

Γ	8				
Q	2	3	4	5	6
$U^{(ess)}$	7	21	35	35	21

Tab. I - G. Oliveri and L. Poli, "Optimal Sub-Arraying of Compromise Planar ..."

	w_1	w_2	w_3	w_4	w_5
$H-WG-ACO$	1.0942	2.0305	2.9870	4.5573	5.6723
$H-BEM$	1.0488	2.7605	4.2845	4.8999	5.5077

Tab. II - G. Oliveri and L. Poli, "Optimal Sub-Arraying of Compromise Planar ..."